D1-2001-283

INCLUSIVE PRODUCTION OF ANTIHYPERONS IN *nC* INTERACTIONS

EXCHARM Collaboration:
Dubna – Almaty – Bucharest – Minsk –
Moscow – Sofia – Tbilisi

Submitted to «European Physical Journal C»

A. N. Aleev, V. P. Balandin, E. A. Goudzovski, D. K. Guriev, P. Hristov,
I. M. Ivanchenko, Z. M. Ivanchenko, M. N. Kapishin, N. N. Karpenko,
V. D. Kekelidze, Z. I. Kozhenkova, V. V. Koren'kov, I. G. Kosarev,
N. A. Kuzmin, A. L. Lyubimov, D. T. Madigojine, V. G. Mazny,
A. S. Mestvirishvili, N. A. Molokanova, A. N. Morozov, Yu. K. Potrebenikov,
L. A. Slepets, V. N. Spaskov, G. T. Tatishvili, V. V. Trofimov, I. P. Yudin,
A. I. Zinchenko
Joint Institute for Nuclear Research, Dubna, Russia

A. P. Bugorski
Institute of High Energy Physics, Protvino, Russia

A. A. Loktionov
Institute of Physics and Technology, Almaty, Kazakhstan

T. Ponta, T. Preda
Institute of Atomic Physics, Bucharest, Romania

I. M. Geshkov
Institute for Nuclear Research and Nuclear Energy, Sofia, Bulgaria

N. S. Amaglobeli, M. V. Kopadze, R. A. Kvatadze, N. L. Lomidze
High Energy Physics Institute, Tbilisi State University, Georgia

T. S. Grigalashvili
Institute of Physics, Georgian Academy of Sciences, Tbilisi, Georgia

1 Introduction

Existing experimental data on antihyperon production by nucleons were obtained mainly in proton beams [1 – 12]. Only few measurements were performed in neutron beams [13, 14]. It is still a question weather characteristics of antihyperon production by protons and neutrons are similar. New data on antihyperon production can provide additional information about hadron interactions.

In this paper the results on antihyperon inclusive production in neutron-carbon interactions obtained in the EXCHARM experiment at the Serpukhov accelerator are presented.

Antihyperons were identified by their essential decays:

$$\bar{\Lambda}^0 \to \bar{p}\pi^+, \tag{1}$$

$$\begin{aligned} \bar{\Sigma}(1385)^- &\to \bar{\Lambda}^0\pi^- \\ &\hookrightarrow \bar{p}\pi^+, \end{aligned} \tag{2}$$

$$\begin{aligned} \bar{\Sigma}(1385)^+ &\to \bar{\Lambda}^0\pi^+ \\ &\hookrightarrow \bar{p}\pi^+, \end{aligned} \tag{3}$$

$$\begin{aligned} \bar{\Xi}^+ &\to \bar{\Lambda}^0\pi^+ \\ &\hookrightarrow \bar{p}\pi^+. \end{aligned} \tag{4}$$

2 The EXCHARM experiment

The EXCHARM setup is placed in the neutron beam (channel 5N) of the Serpukhov accelerator. Beam neutrons are produced on the internal beryllium target by 70 GeV primary protons at zero angle to the proton orbit. The target is followed by a set of collimators and a lead filter of remotely controlled thickness up to 20 cm for γ rejection. Charged particles are swept out of the beam by accelerator magnets and a special sweeping magnet SP-129 installed at the exit of the final collimator. The neutron energy [15] ranges from 20 GeV to 70 GeV. The mean energy of the beam is $\sim$ 51 GeV (fig. 1).

The layout of the EXCHARM setup is presented in fig. 2. The detector is described in the right coordinate system with OZ axis directed along the neutron beam, and OY axis directed vertically up. The centre of coordinate system coincides with the centre of the analysing dipole magnet SP-40A.

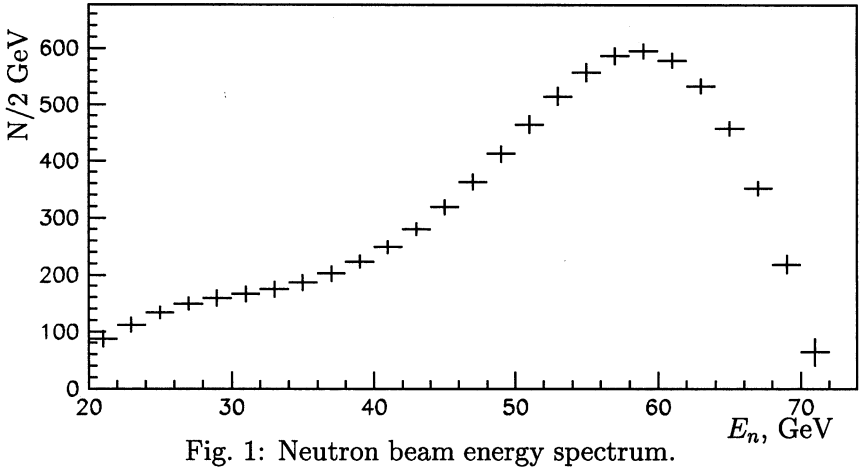

Fig. 1: Neutron beam energy spectrum.

The magnet aperture is 274×49 cm^2. Magnetic field is directed along the OY axis, and has maximum value of ≈ 0.79 T. Polarity of the field was alternated every 5–6 hours during the data taking. The magnet causes a transverse momentum kick of ≈ 0.45 GeV/c.

Neutrons were interacting with the 1.3 g/cm^2 (1.5 cm) long carbon target (T) located in front of the spectrometer. Produced charged particles were detected by 11 proportional chambers (PC) with 2 mm wire spacing. Eight chambers upstream the magnet (PC 1–8) have two coordinate planes each. Two of the PC's have wire orientation $\pm 22.5°$ with respect to vertical plane, the others have horizontal and vertical wire orientation. Three chambers downstream of the magnet (PC A–C) have three coordinate planes each. The wire orientations of three planes are horizontal, vertical and $-22.5°$ with respect to vertical plane. Charged track momentum resolution of the spectrometer is $\sigma_p/p = 10^{-3} \cdot \sqrt{0.65 \cdot p^2 + 34.55}$, where p is expressed in GeV/c.

Two scintillator hodoscopes $H1$ and $H2$ consisting of 15 and 60 counters, respectively, are used to form the trigger signal. Two multichannel threshold gas Cherenkov counters $C1$ and $C2$ filled with freon and air, respectively, under atmospheric pressure, are intended to separate charged hadrons ($p(\bar{p})$, $K^{\pm}$, $\pi^{\pm}$).

The trigger was designed as a coincidence of signals from the hodoscopes $H1$ and $H2$, hodoscopic strips of three PC planes, and anti-counter A. Trigger requirement selected events with at least four charged particles

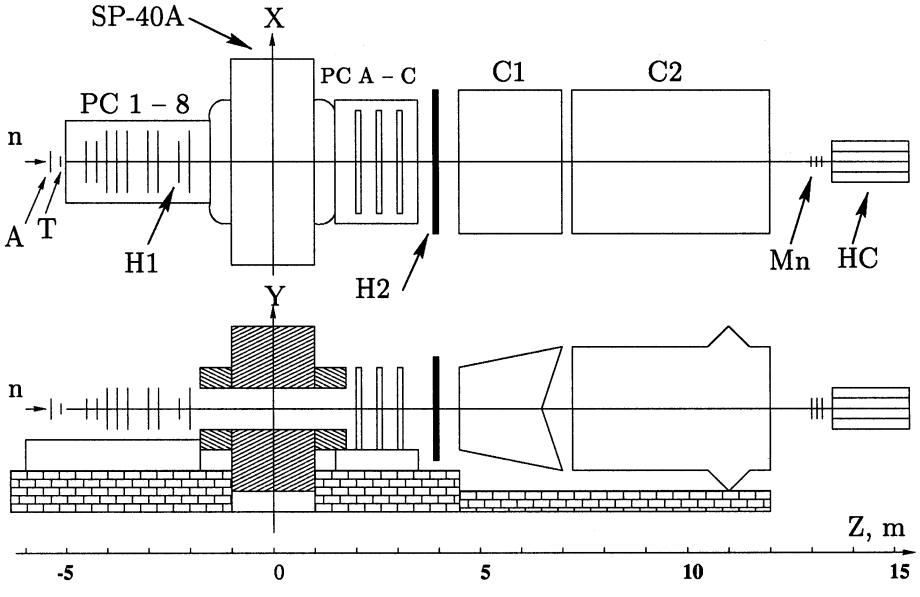

Fig. 2: The EXCHARM spectrometer.

passing through the spectrometer.

More detailed description of the apparatus can be found elsewhere [16].

3 Event selection

The presented results are based on the analysis of $\sim 1.84 \times 10^8$ nC interactions. Experimental events have been processed by BISON program [17] to reconstruct tracks of charged particles and to define their parameters. To select the events with a particular topology and to perform physical and statistical analysis, the program BISMXC [18] was implemented.

3.1 $\bar{\Lambda}^0$ identification

$\bar{\Lambda}^0$'s were selected by their decay (1) which corresponds to the so called neutral vertex topology. A neutral vertex consists of a pair of oppositely charged reconstructed tracks. The closest distance of approach (CDA) of these tracks should not exceed 0.5 cm, which excludes $\sim$17% of all the possible candidates. To reduce the background caused by interactions in the target it is required that Z coordinate of the decay vertex $Z_{\bar{\Lambda}}$ occupies

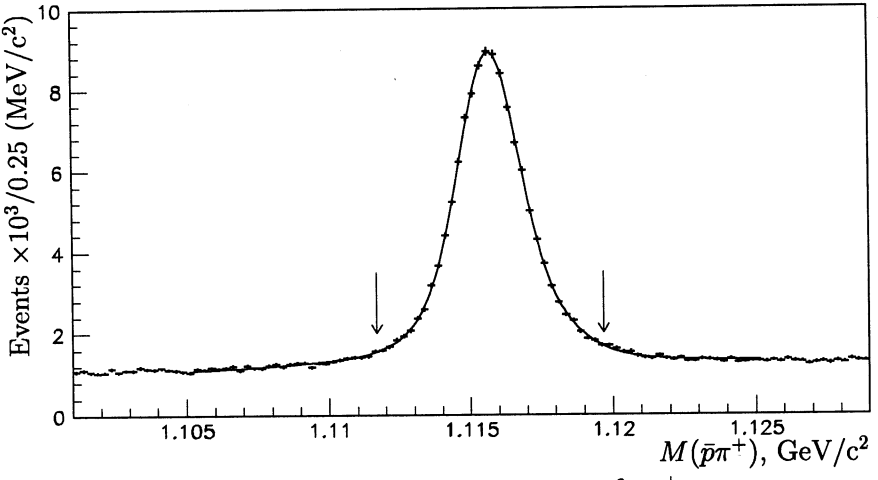

Fig. 3: Effective mass spectrum of $\bar{p}\pi^+$.

the region situated at the distance at least 10 cm downstream the target:

$$Z_{\bar{\Lambda}} - (Z_T + \frac{1}{2}L_T) > 10 \text{ cm}, \tag{5}$$

where $Z_T = -460$ cm is the coordinate of the target centre, and $L_T = 1.5$ cm is the target thickness. The criterion has been selected to minimise the relative error of the number of events in the signal. This condition decreases background by a factor of ~ 2 while removing only $\sim 10\%$ of the signal.

The lower limit of the probability of antiproton hypothesis for the negatively charged track calculated on the basis of the data from Cherenkov detectors was chosen so as to exclude safely identified π^- and K^-. That allows to decrease background by a factor of ~ 11.5 removing only $\sim 16\%$ of the signal.

Thus, about $0.65{\cdot}10^6$ combinations have been selected. The $\bar{p}\pi^+$ effective mass distribution for the selected pairs of tracks is shown in fig. 3. A clear signal of $\bar{\Lambda}^0$ decay (1) is seen in the spectrum. The background is caused mainly by combinations of reconstructed charged particles produced in the target ($\approx 40\%$), and in the air within the spectrometer ($\approx 60\%$). The spectrum was approximated using a MINUIT [19] minimisation routine by a sum of three Gaussian functions describing the signal and a linear function for the background. The reason for introduction of several Gaussians is dependence of experimental mass resolution on $\bar{\Lambda}^0$ momentum. Three

Gaussian functions are the minimal number necessary to obtain satisfactory quality of approximation: $\chi^2/\mathrm{ndf}=1.2$. Mass resolution was calculated as a root-mean-square of the three Gaussian widths obtained from the fit weighted by the corresponding Gaussian amplitudes: $\sigma = 1.38$ MeV/c^2. Event was identified as a candidate to $\bar{\Lambda}^0$ decay if the effective mass $M(\bar{p}\pi^+)$ is within 4 MeV/c^2 from the nominal mass $M_{\bar{\Lambda}}$:

$$\left|M(\bar{p}\pi^+) - M_{\bar{\Lambda}}\right| < 4 \text{ MeV/c}^2, \tag{6}$$

which is close to treble average resolution. The selected mass interval is marked with vertical arrows in fig. 3.

These requirements leave about $0.14 \cdot 10^6$ candidates to the decay (1). The number of observed events was calculated by integration of the Gaussian part of the approximating function, and equals $0.10 \cdot 10^6$. The number of events in background was calculated by integration of the background function within the interval ± 4 MeV/c^2 from the nominal mass, and equals $0.04 \cdot 10^6$.

Characteristics of the obtained $\bar{\Lambda}^0$ signal are presented in tab. 1.

Tab. 1: Characteristics of antihyperon signals.

Decay	Mass [MeV/c^2]	σ [MeV/c^2]	Γ [MeV/c^2]	Number
$\bar{\Lambda}^0 \to \bar{p}\pi^+$	1115.7 ± 0.3	1.4 ± 0.1	—	100300 ± 440
$\bar{\Sigma}(1385)^- \to \bar{\Lambda}^0\pi^-$	1380.0 ± 1.4	—	31.7 ± 3.4	1760 ± 180
$\bar{\Sigma}(1385)^+ \to \bar{\Lambda}^0\pi^+$	1380.0 ± 2.1	—	35.9 ± 7.6	1180 ± 190
$\bar{\Xi}^+ \to \bar{\Lambda}^0\pi^+$	1321.8 ± 0.8	1.71 ± 0.04	—	1020 ± 40

3.2 $\bar{\Sigma}(1385)^{\pm}$ resonance identification

The candidates to the decays (2) and (3) of $\bar{\Sigma}(1385)^{\mp}$ were searched for in combinations of $\bar{\Lambda}^0$ candidates with each of the additional negative (positive) tracks. The CDA of the reconstructed $\bar{\Lambda}^0$ trajectory and the additional track should not exceed 0.2 cm. The point of closest approach of the $\bar{\Lambda}^0$ trajectory and the additional track is considered as the resonance decay vertex. Z coordinate of this vertex $Z_{\bar{\Sigma}}$ should be situated within double experimental resolution ($\sigma_Z = 1$ cm) from the edges of the target:

$$|Z_{\bar{\Sigma}} - Z_T| < \frac{1}{2}L_T + 2\sigma_Z. \tag{7}$$

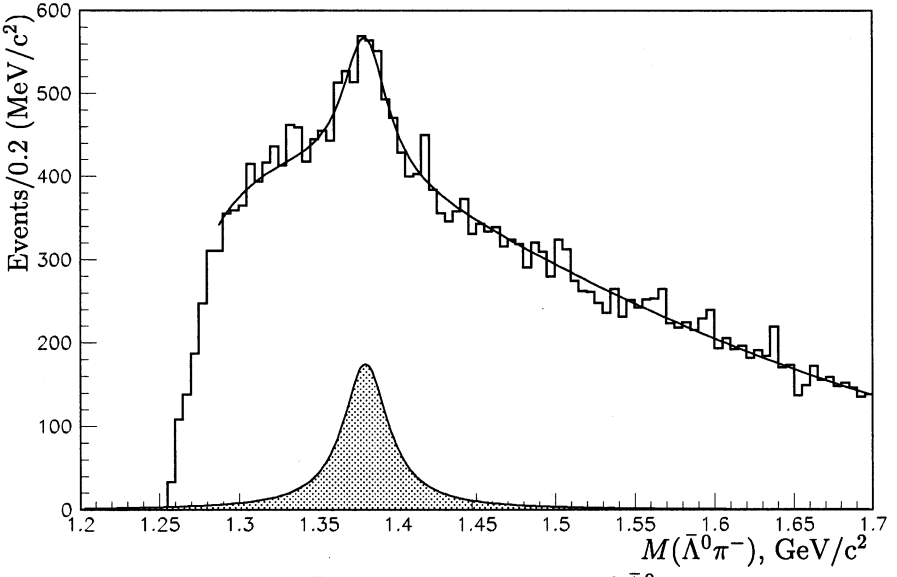

Fig. 4: Effective mass spectrum of $\bar{\Lambda}^0\pi^-$.

About $33 \cdot 10^3$ candidates to the decay (2) and $46 \cdot 10^3$ candidates to the decay (3) have been selected. The effective mass spectra of $\bar{\Lambda}^0\pi^-$ and $\bar{\Lambda}^0\pi^+$ hypotheses for the selected combinations are shown in fig. 4 and 5, respectively. Wide signals in these spectra correspond to the decays (2) and (3). Background is caused mainly by combinatorics. The spectra of $\bar{\Lambda}^0\pi^-$ and $\bar{\Lambda}^0\pi^+$ effective mass were approximated by the functions

$$\left(\frac{dN}{dM}\right)_- = BG(M) + BW(M), \tag{8}$$

and

$$\left(\frac{dN}{dM}\right)_+ = BG(M) + BW(M) + G(M), \tag{9}$$

respectively. Here the background is described by a smooth function which responds to the production threshold (M_{thres}):

$$BG(M) = b_1(M - M_{thres})^{b_2} \exp(b_3 M + b_4 M^2), \quad M > M_{thres}, \tag{10}$$

where b_1, ..., b_4 are free parameters. The signal is approximated by a relativistic Breit-Wigner function

$$BW(M) = \frac{AMM_0\Gamma_R}{(M^2 - M_0^2)^2 + M_0^2\Gamma_R^2}, \tag{11}$$

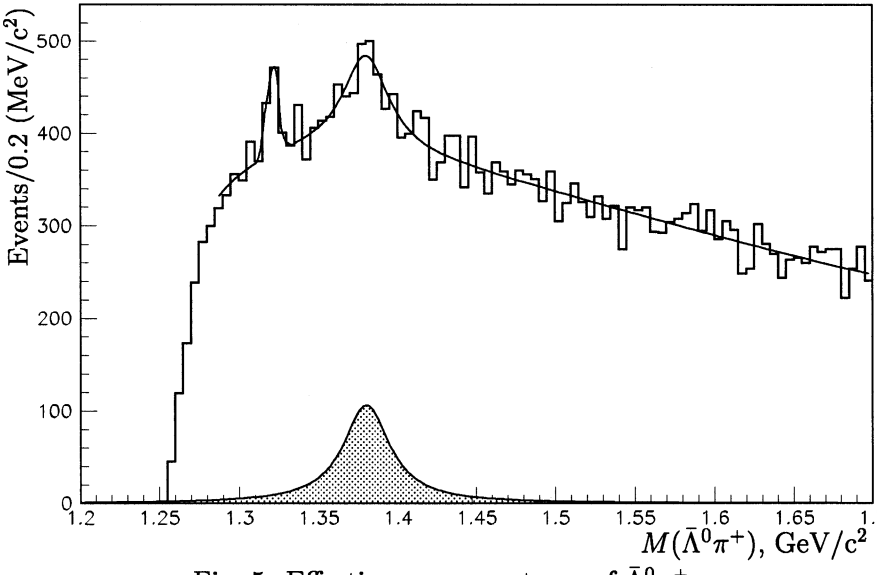

Fig. 5: Effective mass spectrum of $\bar{\Lambda}^0\pi^+$.

where the free parameters are: A – scale factor, M_0 – position of the resonance maximum, and Γ_R – resonance width. A Gaussian function $G(M)$ is applied in the $\bar{\Sigma}(1385)^+$ case to account for a peak in the spectrum produced by $\bar{\Xi}^+ \to \bar{\Lambda}^0\pi^+$ decays occurring within or near the target (see fig. 5). The amounts of detected resonances were calculated by analytical integration of the Breit-Wigner parts of the functions (8) and (9). Analytical integration allows to calculate the errors of the numbers of events taking into account the errors of the parameters of the approximating functions. Characteristics of the obtained $\bar{\Sigma}(1385)^{\pm}$ signals are presented in tab. 1.

3.3 $\bar{\Xi}^+$ identification

To search for the candidates to the $\bar{\Xi}^+$ decay (4), $\bar{\Lambda}^0$ candidates were combined with each of the additional positive tracks. The CDA of the reconstructed $\bar{\Lambda}^0$ trajectory and the additional track should not exceed 0.5 cm. The point of their closest approach is considered as the decay vertex. To reduce the background caused by interactions in the target, it is required that Z coordinate of the decay vertex $Z_{\bar{\Xi}}$ is situated at least

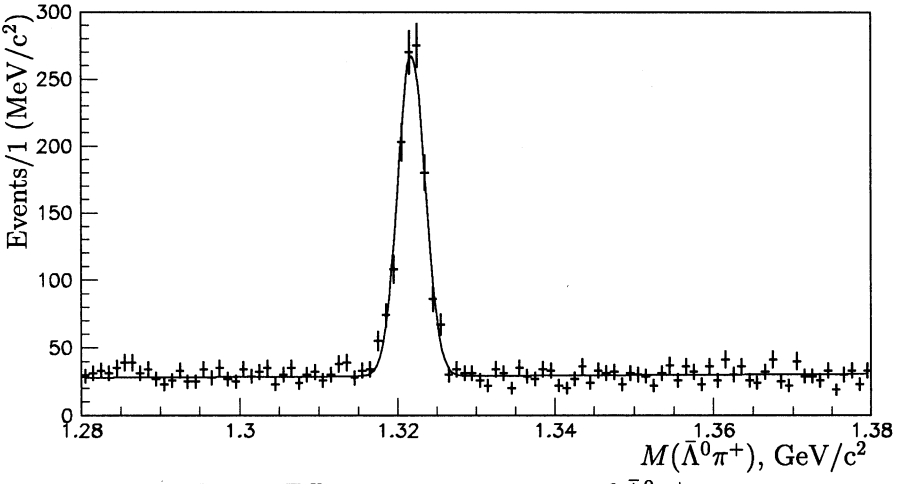

Fig. 6: Effective mass spectrum of $\bar{\Lambda}^0\pi^+$.

10 cm downstream the target:

$$Z_{\bar{\Xi}} - (Z_T + \frac{1}{2}L_T) > 10 \text{ cm}. \tag{12}$$

For further reduction of background, it is required that the distance between $\bar{\Lambda}^0$ and $\bar{\Xi}^+$ decay vertices along the beam axis should be greater than 5 cm:

$$Z_{\bar{\Xi}} - Z_{\bar{\Lambda}} > 5 \text{ cm}. \tag{13}$$

About $15 \cdot 10^3$ candidates to the decay (4) have been selected. The $\bar{\Lambda}^0\pi^+$ effective mass spectrum of the selected combinations is shown in fig. 6. A clear signal of $\bar{\Xi}^+$ decay (4) is seen in the spectrum. The spectrum was approximated by a sum of a Gaussian function describing the signal, and a linear function for the background. The number of observed decays was calculated by integration of the Gaussian part of the approximating function. Characteristics of the obtained signal are presented in tab. 1.

Measured masses of $\bar{\Lambda}^0$ and $\bar{\Xi}^+$ coincide within the errors with the nominal ones of the PDG [20]. Measured masses of $\bar{\Sigma}(1385)^{\pm}$ resonances are slightly lower than the nominal ones: the corresponding deviations are 2.8 MeV/c^2 for $\bar{\Sigma}(1385)^-$, and 7.2 MeV/c^2 for $\bar{\Sigma}(1385)^+$. Measured widths of the resonances coincide with the nominal ones.

4 Antihyperon production characteristics

Overall and differential acceptances have been calculated by a Monte-Carlo simulation. The events were generated in such a way that for each considered antihyperon $\bar{H}$ the corresponding hyperon H was chosen as an accompanying particle:

$$n + N \to \bar{H} + H + X. \tag{14}$$

Here X represents the set of accompanying particles generated by JETSET [21] in accordance with the conservation laws.

A GEANT based program [22] was used to trace the particles through the experimental setup. The simulated data were treated by the same reconstruction and analysis programs that were used to process the experimental data.

Inclusive production cross-section has been parametrised in accordance with the quark counting rules [23, 24]:

$$\frac{d^2\sigma}{dx_F dp_t^2} \sim (1 - |x_F|)^n \cdot \exp(-bp_t^2). \tag{15}$$

Here $x_F = p_l^*/p_l^{max}$ is the Feynman variable, p_l^* is longitudinal momentum of the studied particle, p_l^{max} is its maximal possible momentum (p_l^* and p_l^{max} are defined in neutron-nucleon centre of mass system), p_t is its transverse momentum.

To obtain the experimental values of production parameters n and b, simulation is carried out for various values of parameters, and normalised p_l and p_t^2 spectra of reconstructed antihyperons obtained for experimental and simulated events are compared by the χ^2 criterion. (Here p_l is longitudinal momentum of antihyperon in the laboratory frame.) The obtained values of parameters correspond to the minimum of χ^2. Errors of parameters are calculated in accordance with the method of multi-parameter error calculation described in [19].

It is expected that cross-section parametrisation (15) is valid only at the values of x_F corresponding to the fragmentation region, while in the central region differential cross-section behaves differently. A possible way to estimate the x_F region in which parametrisation (15) is valid is determination of the parameter n by the above method in various regions of the Feynman variable $x_F > \widetilde{x_F}$, gradually increasing the lower boundary of the region $\widetilde{x_F}$.

Energy of incident neutron is unknown in every single experimental event, since the neutron beam is not monochromatic. Hence the value of x_F can not be obtained, and it is impossible to apply the same x_F cut to the experimental events. Therefore, to provide the same conditions of analysis for experimental and MC events, which must be done to justify comparison of experimental and simulated momentum spectra, an appropriate cut on the longitudinal momentum p_l is applied to both MC and experimental events. The cut $p_l > \widetilde{p_l}$ is used to ensure that the majority of the accepted events are in the chosen x_F region:

$$p_l > \widetilde{p_l} \quad \Rightarrow \quad x_F > \widetilde{x_F}. \tag{16}$$

The value of $\widetilde{p_l}$ corresponding to a certain value of $\widetilde{x_F}$ is defined by analysing the p_l vs x_F plot of the accepted MC events simulated in the whole kinematic region $-1 \leq x_F \leq 1$.

To estimate the region of validity of the parametrisation (15), inclusive cross-section parameters for $\bar{\Lambda}^0$ have been obtained in 9 various regions of the Feynman variable: $x_F > \widetilde{x_F}$. The lower boundary of the interval $\widetilde{x_F}$ has been varied from 0.0 to 0.4 with the step of 0.05. The values of the parameters n and b obtained for various $\widetilde{x_F}$ are presented in fig. 7. Discretisation of values and errors is due to the fact that the parameters have been varied with the steps $\Delta n = 0.1$ and $\Delta b = 0.1$ $(\mathrm{GeV/c})^{-2}$ in Monte-Carlo simulation.

The obtained dependence of n on x_F explicitly indicates two kinematic regions with different properties of differential cross-section. The stability of n for $\widetilde{x_F} \geq 0.1$ allows to conclude that differential cross-section is well described by the parametrisation (15) in the region $x_F > 0.1$, which corresponds to the fact that contribution of soft processes becomes dominant in this region. On the other hand, significant deviations from the used model are revealed in the region $0 < x_F < 0.1$. The behaviour of the parameter b is also stable in the region $x_F > 0.1$ (fig.7).

In order to minimise model dependence of the results, measurement of parameters and cross-sections of antihyperon production has been carried out in the kinematic region of model validity (RMV). In accordance with the obtained results, the RMV has been defined as $x_F > 0.1$ for $\bar{\Lambda}^0$. The same condition has been chosen for all the other studied antihyperons.

The p_l vs x_F plot for accepted $\bar{\Lambda}^0$'s simulated in the whole kinematic region is presented in fig. 8. It justifies the choice of the region in which $\widetilde{x_F}$ has been varied, and shows an example of determination of momentum

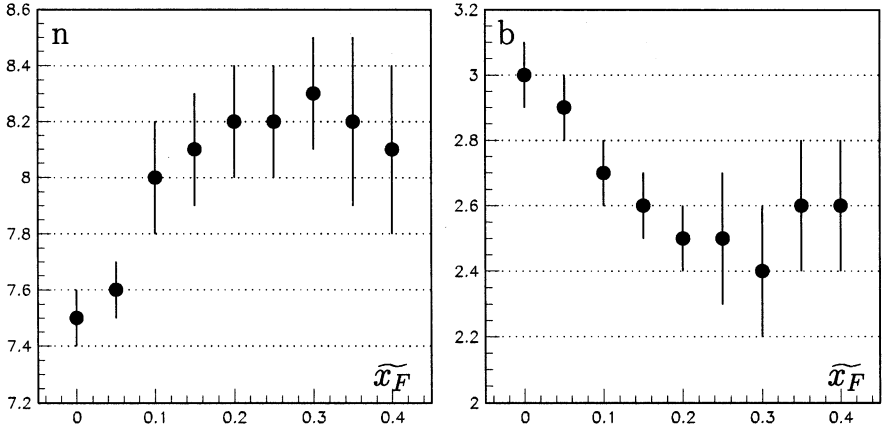

Fig. 7: $\bar{\Lambda}^0$ production parameters n and b at various $\widetilde{x_F}$.

cut boundary $\widetilde{p_l}$ on the basis of the Feynman variable cut boundary $\widetilde{x_F}$ for the chosen RMV $x_F > 0.1$.

The values of lower p_l cut boundaries, production parameters obtained in the RMV, their errors, and corresponding minimal χ^2's per number of degrees of freedom for each antihyperon under consideration are presented in tab. 2. As an example, normalised experimental and simulated p_l and p_t^2 spectra for $\bar{\Lambda}^0$ obtained in the RMV at minimal χ^2 are presented in fig. 9. The spectra obtained from the simulation are in good agreement with the experimental ones.

Quark counting model [23, 24] predicts the value of the parameter $n = 5$ for all the studied antihyperons. Obtained values of n parameter for $\bar{\Sigma}(1385)^{\pm}$ are compatible with this prediction, while the values for $\bar{\Lambda}^0$ and $\bar{\Xi}^+$ are higher than the predicted ones.

Comparison of the obtained values of production parameters for $\bar{\Lambda}^0$ and $\bar{\Xi}^+$ with the other experimental data obtained in nucleon-nucleon interactions is presented in tab. 3 and 4. The results are in good agreement. Production parameters for $\bar{\Sigma}^{\pm}(1385)$ in nucleon-nucleon interactions have been measured for the first time.

Tab. 2: Production parameters in the region $x_F > 0.1$.

State	$\widetilde{p_l}$, GeV/c^2	n	$\chi^2_{p_l}$/ndf	b, (GeV/c)$^{-2}$	$\chi^2_{p_t^2}$/ndf
$\bar{\Lambda}^0$	12	8.0 ± 0.2	1.00	2.7 ± 0.1	0.93
$\bar{\Sigma}(1385)^-$	13	5.3 ± 0.3	0.67	2.4 ± 0.2	0.38
$\bar{\Sigma}(1385)^+$	14	5.0 ± 0.4	0.51	2.7 ± 0.2	0.25
$\bar{\Xi}^+$	13	7.5 ± 1.0	0.22	2.8 ± 0.3	0.89

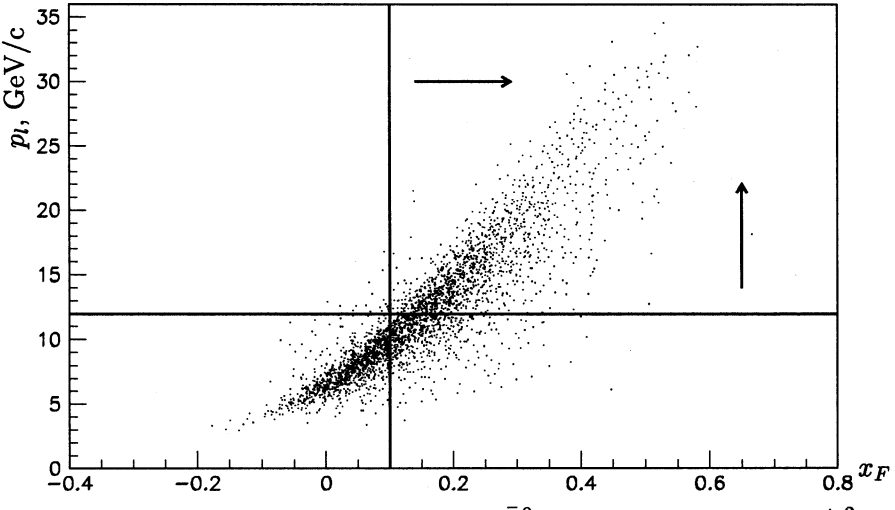

Fig. 8: p_l vs x_F for accepted simulated $\bar{\Lambda}^0$'s. $\widetilde{x_F}$=0.1, $\widetilde{p_l}$=12 GeV/c^2.

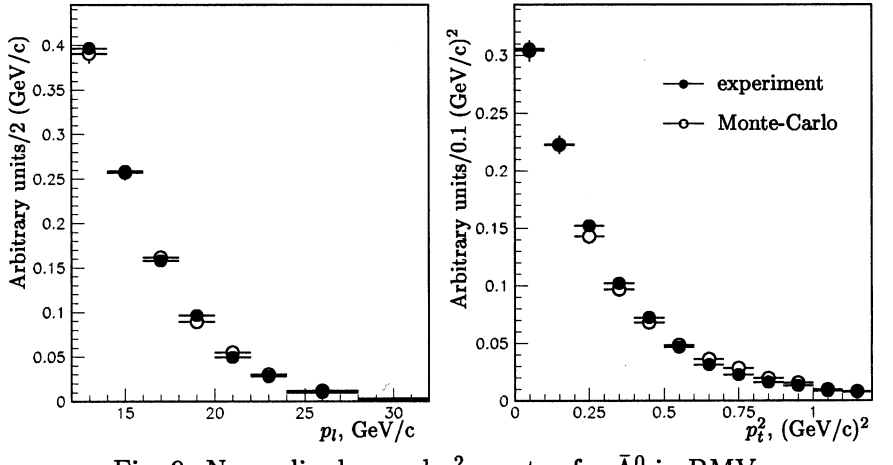

Fig. 9: Normalised p_l and p_t^2 spectra for $\bar{\Lambda}^0$ in RMV.

Tab. 3: Production parameters for $\bar{\Lambda}^0$ in nucleon-nucleon interactions.

Reference	Interaction	E_{beam}	n	b, $(\mathrm{GeV/c})^{-2}$	x_F region
EXCHARM	nN	57 GeV	8.0 ± 0.2	2.7 ± 0.1	$x_F > 0.1$
[3]	pN	147 GeV		3.2 ± 0.1	whole
[14]	nN	260 GeV	8.0	3.0	$x_F > 0.1$
[8]	pp	405 GeV		3.7 ± 1.3	$x_F > 0$
[10]	pp	1500 GeV	7.1	3.8	$x_F > 0.2$

Tab. 4: Production parameters for $\bar{\Xi}^+$ in nucleon-nucleon interactions.

Reference	Interaction	E_{beam}	n	b, $(\mathrm{GeV/c})^{-2}$	x_F region
EXCHARM	nN	57 GeV	7.5 ± 1.0	2.8 ± 0.3	$x_F > 0.1$
[14]	nN	260 GeV	6 ± 2	2.5 ± 1.0	$x_F > 0.1$

5 Calculation of production cross-sections

5.1 Cross-sections in the region of model validity

Inclusive production cross-sections of antihyperons in the RMV were calculated by the formula

$$\sigma_{nC} = \frac{N_s \cdot A}{M_n \cdot N_A \cdot L_T \cdot \varepsilon \cdot Br}, \tag{17}$$

where N_s – the number of events in the signal; $A = 12$ – target nucleus atomic weight; $M_n = (2.43 \pm 0.14) \cdot 10^{11}$ – the number of neutrons that had passed through the target (neutron monitor); N_A – Avogadro constant; $L_T = 1.3$ g/cm^2 – target thickness; ε – overall efficiency of decay acception and selection; Br – branching ratio of a considered decay channel [20].

The number of events in the signal N_s is defined as described in section 3, but with an additional criterion on longitudinal momenta applied: $p_l > \widetilde{p_l}$. The efficiency ε is obtained from the Monte-Carlo simulation with the previously defined values of production parameters n and b. The number of events in the signal (N_s), event losses due to p_l cut, and overall efficiency (ε) for the considered decays are presented in tab. 5.

Calculated cross-sections of antihyperon inclusive production on carbon nuclei in the RMV are presented in tab. 6. Statistical errors are caused by the errors of experimental signals, which are presented in tab. 5. Systematic errors include uncertainties of neutron monitor M_n, overall efficiency ε, and decay branching [20] combined in quadrature.

The error of efficiency is composed of MC signal error, and systematic uncertainty. The latter is calculated by two methods. According to the first method, the error is calculated as the variation of efficiency at various values of parameters n and b within their errors. According to the second method, the error is calculated as the variation of efficiency when the MC events are weighted with weights depending on p_l. The weights are varied independently in each p_l interval so as to vary the normalised p_l spectrum of accepted simulated events within the errors of the normalised experimental p_l spectrum. The two methods obtain close results: for all the studied antihyperons at various selection criteria the two estimations of systematic error do not differ by more than 1.7 times. The errors of ε presented in tab. 5 are obtained as quadratic sums of statistical and systematic errors.

To calculate cross-section per nucleon σ_{nN}, it was assumed that cross-

Tab. 5: Numbers of decays and efficiencies of registration.

Decay	Number, N_s	Loss at p_l cut	ε, %
$\bar{\Lambda}^0 \to \bar{p}\pi^+$	41100 ± 290	59%	2.28 ± 0.19
$\bar{\Sigma}(1385)^- \to \bar{\Lambda}^0\pi^-$	1186 ± 179	32%	0.91 ± 0.04
$\bar{\Sigma}(1385)^+ \to \bar{\Lambda}^0\pi^+$	830 ± 275	30%	0.79 ± 0.05
$\bar{\Xi}^+ \to \bar{\Lambda}^0\pi^+$	724 ± 34	29%	0.76 ± 0.05

Tab. 6: Cross-sections per carbon nucleus in the region $x_F > 0.1$.

State	σ_{nC} [μb]				
$\bar{\Lambda}^0$	178.0	$\pm$	1.2 (stat)	$\pm$	17.8 (syst)
$\bar{\Sigma}(1385)^-$	14.6	$\pm$	2.2 (stat)	$\pm$	1.1 (syst)
$\bar{\Sigma}(1385)^+$	11.8	$\pm$	3.9 (stat)	$\pm$	1.0 (syst)
$\bar{\Xi}^+$	9.4	$\pm$	0.5 (stat)	$\pm$	0.8 (syst)

Tab. 7: Cross-sections per nucleon in the region $x_F > 0.1$.

State	σ_{nN} [μb]				
$\bar{\Lambda}^0$	34.0	$\pm$	0.2 (stat)	$\pm$	3.4 (syst)
$\bar{\Sigma}(1385)^-$	2.8	$\pm$	0.4 (stat)	$\pm$	0.2 (syst)
$\bar{\Sigma}(1385)^+$	2.3	$\pm$	0.7 (stat)	$\pm$	0.2 (syst)
$\bar{\Xi}^+$	1.8	$\pm$	0.1 (stat)	$\pm$	0.2 (syst)

section is proportional to the geometrical cross-section of the nucleus, i.e. the A-dependence is $\sigma_{nC} = \sigma_{nN} \cdot A^{2/3}$, which is common for soft processes at high x_F. Cross-sections per nucleon in the region $x_F > 0.1$ are presented in tab. 7.

5.2 Comparison with the other results

Additive quark model yields the following relations for the total cross-sections of inclusive production for every antihyperon under consideration:

$$\sigma_{nN}(\bar{H}) \approx \sigma_{pN}(\bar{H}) \approx \sigma_{pp}(\bar{H}), \tag{18}$$

which allows to compare the obtained results with the results of the other experiments in proton and neutron beams.

Extrapolation of cross-sections from the RMV into the whole kinematic region on the basis of the obtained information could be only approximate, as the behaviour of differential cross-section outside the RMV is unknown. To fulfil the goal of comparison of our results with the other data, the extrapolation has been produced taking into account theoretical considerations, and the results of the other experiments.

Theoretically the shape of differential cross-section should be symmetric in forward and backward hemispheres, and this assumption is really used for extrapolation into the whole kinematic region in [3 – 8, 13]. Furthermore, in [3] and [11] it is shown that in the central region $0 < |x_F| < 0.1$ differential cross-section is increasing as $|x_F|$ is decreasing, though it is demonstrated in [9, 10] and also in the present investigation (fig. 7) that its slope in the central region is less steep than given by the parametrisation (15).

In correspondence with these data, extrapolation of cross-sections into the whole kinematic region has been carried out under assumption that differential cross-section is a symmetric function of x_F. The lower limit for

Tab. 8: Total cross-sections per nucleon.

State	σ_{nN} [μb]						
$\bar{\Lambda}^0$	154.0	$\pm$	1.2(stat)	$\pm$	17.6(syst)	$\pm$	18.0(model)
$\bar{\Sigma}(1385)^-$	10.2	$\pm$	1.6(stat)	$\pm$	0.8(syst)	$\pm$	0.6(model)
$\bar{\Sigma}(1385)^+$	8.2	$\pm$	2.8(stat)	$\pm$	0.7(syst)	$\pm$	0.5(model)
$\bar{\Xi}^+$	7.9	$\pm$	0.4(stat)	$\pm$	0.7(syst)	$\pm$	0.9(model)

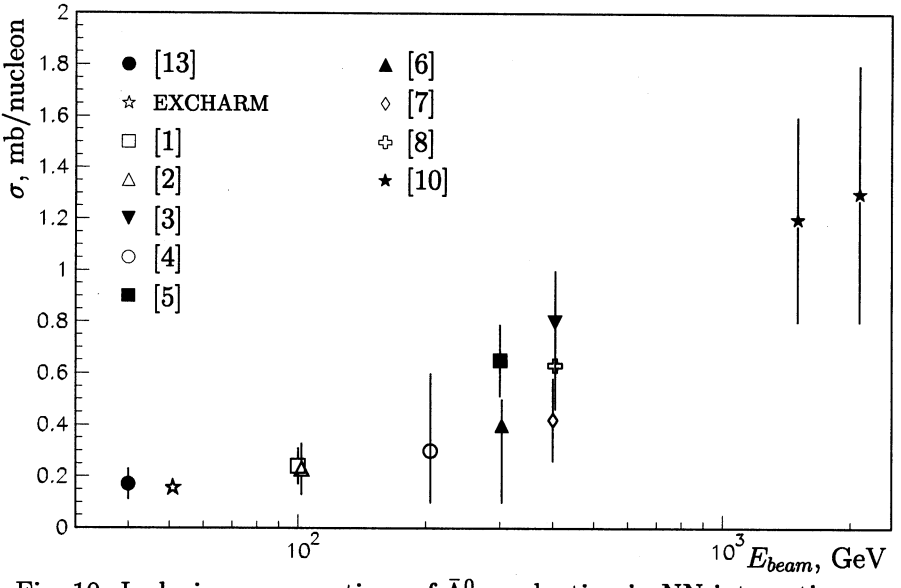

Fig. 10: Inclusive cross-sections of $\bar{\Lambda}^0$ production in NN-interactions.

total cross-section has been estimated under assumption that differential cross-section is a flat function of x_F in the region $0 < x_F < 0.1$. The upper limit has been calculated assuming that differential cross-section obeys the parametrisation (15). For extrapolation the value of the parameter n has been taken from the RMV for $\bar{\Xi}^+$ and $\bar{\Sigma}(1385)^{\pm}$, and has been defined in the region $x_F > 0$ for $\bar{\Lambda}^0$ (fig. 7). The extrapolated cross-sections per nucleon presented in tab. 8 are average values of upper and lower limits. The shown extrapolation errors (model) have been calculated as half of the difference between the limits.

The comparison of the obtained total $\bar{\Lambda}^0$ production cross-section per nucleon with the other results is presented in fig. 10, where statistic, systematic, and extrapolation errors are combined in quadrature. It shows that the present measurement is in good agreement with the other ones, and has the minimal relative error. No data from the other experiments have been found for the other studied antihyperons.

6 Summary

Cross-sections of inclusive production of antihyperons in neutron-carbon interactions at mean neutron energy ~ 51 GeV measured in the kinematic region $x_F > 0.1$ under assumption that differential cross-sections obey the parametrisation (15) are presented in tab. 6. The kinematic region has been chosen as the region of validity of the used parametrisation in order to minimise model dependence of the results. Production cross-sections have been extrapolated into the whole kinematic region, the errors of extrapolation have been calculated (tab. 8).

Cross-sections of $\bar{\Lambda}^0$ and $\bar{\Xi}^+$ production include the ones of $\bar{\Lambda}^0$ and $\bar{\Xi}^+$ produced due to decays of resonances and cascade decays.

Cross-sections of $\bar{\Xi}^+$ and $\bar{\Sigma}(1385)^{\pm}$ production in nucleon-nucleon interactions have been measured for the first time. The obtained total cross-section of $\bar{\Lambda}^0$ production is consistent with the ones measured in the other proton and neutron experiments, and has the minimal relative error.

Parameters n and b of the used parametrisation obtained for each studied antihyperon are presented in tab. 2. The values of the production parameters for $\bar{\Lambda}^0$ and $\bar{\Xi}^+$ are in good agreement with the results of the other experiments. Production parameters for $\bar{\Sigma}(1385)^{\pm}$ have been measured for the first time in nucleon-nucleon interactions. The obtained values of the parameter n for $\bar{\Sigma}(1385)^{\pm}$ coincide with the ones predicted in [23, 24].

The work is supported by the Russian Foundation for Basic Research, project 00-07-90148.

References

[1] M. Alston et al., *Phys.Rev.Lett.*, 35 (1975) 142.

[2] J.W. Chapman et al., *Phys.Lett.*, 47B (1973) 465.

[3] D. Brick et al., *Nucl.Phys.*, B164 (1980) 1.

[4] G. Charlton et al., *Phys.Rev.Lett.*, 30 (1973) 574.

[5] F. LoPinto et al., *Phys.Rev.*, D22 (1980) 573.

[6] F.T. Dao et al., *Phys.Rev.Lett.*, 30 (1973) 1151.

[7] R.D. Kass et al., *Phys.Rev.*, D20 (1979) 605.

[8] H. Kichimi et al., *Phys.Lett.*, 72B (1978) 411.

[9] F.W. Büsser et al., *Phys.Lett.*, 61B (1976) 309.

[10] S. Erhan et al., *Phys.Lett.*, 85B (1979) 447.

[11] V. Blobel et al., *Nucl.Phys.*, B69 (1974) 454.

[12] A. Sheng et al., *Phys.Rev.*, D11 (1975) 1733.

[13] A.N. Aleev et al., *Yad.Fiz.*, 44 (1986) 661.

[14] M. Zavertyaev, *Nucl.Phys B (Proc.Suppl.)*, 93B (2001) 62.

[15] A.N. Aleev et al., *JINR preprint* P13-94-312 (Dubna, 1994).

[16] A.N. Aleev et al., *Instrum.Exp.Tech.*, 42 (1999) 481.

[17] A. Boniushkina et al., *JINR preprint* P1-93-168 (Dubna, 1993).

[18] A.I. Zinchenko et al., *IFVE AN RK*, 92-01 (Alma-Ata, 1992).

[19] F. James, *Minuit Reference Manual*, D506 (CERN, 1994).

[20] D.E. Groom et al., *Eur.Phys.J.*, C15 (2000) 1.

[21] T. Sjöstrand, *Comp. Phys. Comm.*, 82 (1994) 74.

[22] G.A. Aralbaeva et al., *JINR preprint*, P1-93-85 (Dubna, 1993)

[23] V.A. Matveev, R.M. Muradian, A.N. Tavkhelidze,
Theor. Math. Phys., 40 (1979) 329,
Theor. Math. Phys., 40 (1979) 778.

[24] J.F. Gunion, *Phys.Lett.*, 88B (1979) 150.

Received by Publishing Department
on December 27, 2001.

Алеев А. Н. и др. Д1-2001-283
Инклюзивное рождение антигиперонов в nC-взаимодействиях

Измерены сечения инклюзивного рождения антигиперонов $\overline{\Lambda}^0$, $\overline{\Xi}^+$ и $\overline{\Sigma}(1385)^{\pm}$ в нейтрон-углеродных взаимодействиях при средней энергии нейтронов ~ 51 ГэВ. Определены экспериментальные значения параметров n и b использованной параметризации дифференциального сечения $(1-|x_F|)^n \cdot \exp(-bp_t^2)$, где x_F — переменная Фейнмана, p_t — поперечный импульс. Определена кинематическая область применимости параметризации. Проведено сравнение результатов с предсказаниями модели кваркового счета и результатами других экспериментов.

Работа выполнена в Лаборатории физики частиц ОИЯИ.

Препринт Объединенного института ядерных исследований. Дубна, 2001

Aleev A. N. et al. D1-2001-283
Inclusive Production of Antihyperons in nC Interactions

Inclusive production cross-sections of $\overline{\Lambda}^0$, $\overline{\Xi}^+$ and $\overline{\Sigma}(1385)^{\pm}$ have been measured in neutron-carbon interactions at ~ 51 GeV mean energy of neutrons. The parameters n and b of differential cross-section parametrisation $(1-|x_F|)^n \cdot \exp(-bp_t^2)$, where x_F is the Feynman variable, p_t is transverse momentum, have been obtained. The kinematic region of validity of the parametrisation has been defined. The results are compared with the predictions of quark counting rules and other existing experimental data.

The investigation has been performed at the Laboratory of Particle Physics, JINR.

Preprint of the Joint Institute for Nuclear Research. Dubna, 2001

Макет Т. Е. Попеко

Подписано в печать 04.02.2002
Формат 60 × 90/16. Офсетная печать. Уч.-изд. л. 2,02
Тираж 305. Заказ 53090. Цена 2 р. 40 к.

Издательский отдел Объединенного института ядерных исследований
Дубна Московской области